INTERFACE

royalsocietypublishing.org/journal/rsif

Research

Cite this article: Natale CF, Lafaurie-Janvore J, Ventre M, Babataheri A, Barakat AI. 2019 Focal adhesion clustering drives endothelial cell morphology on patterned surfaces. *J. R. Soc. Interface* **16**: 20190263. http://dx.doi.org/10.1098/rsif.2019.0263

Received: 11 April 2019
Accepted: 24 June 2019

Subject Category:
Life Sciences–Engineering interface

Subject Areas:
biomaterials, biomedical engineering, bioengineering

Keywords:
endothelial cells, adhesive micropatterns, substrate topography, focal adhesions, cell morphology, cytoskeleton

Author for correspondence:
C. F. Natale
e-mail: carlo.natale@unina.it

Electronic supplementary material is available online at https://doi.org/10.6084/m9.figshare.c.4638149.

THE ROYAL SOCIETY PUBLISHING

Focal adhesion clustering drives endothelial cell morphology on patterned surfaces

C. F. Natale[1,2], J. Lafaurie-Janvore[1], M. Ventre[2,3], A. Babataheri[1] and A. I. Barakat[1,4]

[1]Hydrodynamics Laboratory, Ecole Polytechnique, CNRS UMR7646, Palaiseau, France
[2]Interdisciplinary Research Centre on Biomedical Materials (CRIB), University of Naples Federico II, Naples 80125, Italy
[3]Department of Chemical, Materials and Industrial Production Engineering, University of Naples Federico II, Italy
[4]School of Mechanical and Manufacturing Engineering, University of New South Wales, Sydney, Australia

CFN, 0000-0002-5413-5184; MV, 0000-0003-3375-9112; AIB, 0000-0002-7551-3631

In many cell types, shape and function are intertwined. *In vivo*, vascular endothelial cells (ECs) are typically elongated and aligned in the direction of blood flow; however, near branches and bifurcations where atherosclerosis develops, ECs are often cuboidal and have no preferred orientation. Thus, understanding the factors that regulate EC shape and alignment is important. *In vitro*, EC morphology and orientation are exquisitely sensitive to the composition and topography of the substrate on which the cells are cultured; however, the underlying mechanisms remain poorly understood. Different strategies of substrate patterning for regulating EC shape and orientation have been reported including adhesive motifs on planar surfaces and micro- or nano-scale gratings that provide substrate topography. Here, we explore how ECs perceive planar bio-adhesive versus microgrooved topographic surfaces having identical feature dimensions. We show that while the two types of patterned surfaces are equally effective in guiding and directing EC orientation, the cells are considerably more elongated on the planar patterned surfaces than on the microgrooved surfaces. We also demonstrate that the key factor that regulates cellular morphology is focal adhesion clustering which subsequently drives cytoskeletal organization. The present results promise to inform design strategies of novel surfaces for the improved performance of implantable cardiovascular devices.

1. Introduction

In cells and tissues, form and function are often intricately intertwined [1–3]. In the vascular system, the endothelial cells (ECs) lining the inner surfaces of blood vessels are generally elongated and aligned in the direction of blood flow, and it has been suggested that this cellular morphology and orientation constitute a form of structural adaptation that optimizes EC function [4,5]. Interestingly, in the vicinity of branches and bifurcations where atherosclerotic lesions preferentially develop, ECs are typically cuboidal and have no preferred orientation [6]. Thus, understanding the factors that regulate EC shape and alignment along with elucidating the relationships between EC shape and function is of great interest.

EC morphology is the result of multiple physical and chemical signals of the cell microenvironment. One physical factor that is known to regulate EC shape, cytoskeletal arrangement and consequently cell function is the local flow field to which the cell's apical surface is subjected [7,8]. However, even in the absence of external fluid shear stress, EC shape impacts cellular function, with cytoskeletal organization actively regulating immunogenic responses and cellular migration profiles [9].

More recently, cell shape and orientation have been shown to also be modulated by lateral walls that physically constrain cellular spreading [10,11] as well as by biophysical cues exerted on the cell's basal surface via substrate patterns that impose directional bias to the cells' focal adhesion (FA) sites [12–15]. In their *in vivo* microenvironment, ECs are anchored to the basement membrane, a specialized extracellular matrix (ECM) whose surface exhibits nano- to micro-scale topographic features [16,17]. Mimicking this topography *in vitro* has been shown to regulate EC shape and function [18–20]. The capability of controlling EC morphology and orientation by substrate engineering, combined with an understanding of form–function relationships, provides exciting opportunities to optimize the design of vascular grafts and endovascular devices to ensure improved haemocompatibility and anti-thrombotic outcomes.

A strategy of substrate patterning for regulating EC shape and function is the implementation of mosaics of bio-adhesive motifs on planar surfaces [21]. As an example, ECM protein islands of controlled size that limit cell spreading have been shown to impact EC proliferation and chromatin condensation [10,11]. Another strategy involves anisotropic grated surfaces with feature sizes in the micrometre range that regulate EC function through the physical modulation of adaptor protein recruitment and FA maturation [22–24]. Beyond the *in vitro* setting, micropatterning of coronary stents has been shown to favourably influence EC function *in vivo*, resulting in decreased neointimal hyperplasia in a porcine coronary injury model [25].

Despite a plethora of studies aimed at analysing which types of patterns are most effective in controlling cellular behaviour, it remains unclear whether or not planar and topographic patterns of similar dimensions are perceived similarly by the cells and thus exert their effects on cellular morphology and function through similar mechanisms. To address this question, we engineered planar surfaces with anisotropic patterning in the form of alternating adhesive/non-adhesive parallel micro-stripes as well as topographic surfaces in the form of micro-ridges/grooves with similar feature dimensions, and we explored the effects of these patterned surfaces on EC elongation, orientation, FA organization and cytoskeletal assembly.

2. Material and methods

2.1. Preparation of planar micropatterned and topographic microgrooved substrates

Polydimethylsiloxane (PDMS) surfaces were cast using Sylgard 184 (Dow Corning, Midland, MI, USA). After thoroughly mixing elastomer base and curing agent at a 10 : 1 weight ratio, the solution was degassed and the mixture poured into polystyrene Petri dishes (Corning, NY, USA) in order to create a smooth PMDS surface. After curing at 70°C for 1 h, the PDMS substrates were cut into 35 mm diameter circular sections. Planar bio-adhesive patterned substrates (µP) containing alternating 5 µm wide adhesive and 5 µm wide non-adhesive stripes were produced using the deep UV protein micropatterning method described elsewhere [26]. Briefly, PDMS surfaces were first activated by exposure to O_2 plasma (Harrick Scientific Products, Pleasantville, NY, USA) for 1 min and then incubated for 1 h with 0.1 mg ml^{-1} poly-L-lysine-g-poly(ethyleneglycol) (PLL(20)-g[3.5]-PEG(2); SuSoS Surface Technology, Dubendorf, Switzerland) in 10 mM HEPES at pH 7.3 for passivation. After washing with distilled water, the treated surface was illuminated with deep UV light (UVO Cleaner; Jelight, Irvine, CA, USA) through a chromium synthetic quartz photomask (Toppan Printing, Tokyo, Japan) for 3 min to selectively burn desired PLL-g-PEG regions.

Microgrooved patterned substrates (µG) were obtained by replica moulding PDMS on silicon masters. The masters consisted of a 1.5 cm^2 area containing parallel and straight channels with a groove and ridge width of 5 µm and a depth of 1 µm. Microgrooved substrates possessing narrower topographic features were also produced. In particular, PDMS surfaces with 2 µm wide ridges and grooves and a 1 µm groove depth (µG-2 µm) as well as 0.7 µm wide ridges and grooves and a 0.25 µm groove depth (µG-0.7 µm) were fabricated by means of replica moulding. Unpatterned smooth PDMS substrates served as controls for all patterned surfaces. Moreover, to produce microgrooved surfaces with comparable chemical and mechanical properties to the planar bio-adhesive patterned surfaces (µG*), µG substrates were first passivated as described above and then exposed to deep UV light for 3 min without any photomask. Fluorescent imaging of PLL(20)-g[3.5]-PEG(2)-FITC was used to assess the effectiveness of the burning process.

Microcontact printing was used to produce a second category of microgrooved substrate on which fibronectin adhesive proteins were selectively adsorbed onto the ridges but not onto the grooves. This yielded a microstructured surface (µG-FnR) with similar adhesive regions to the µP substrate. To produce the µG-FnR substrates, a smooth PDMS stamp was immersed for 1 h at room temperature in a solution containing rhodamine-conjugated fibronectin (Cytoskeleton, Denver, CO, USA) and bare fibronectin (final concentration of 50 µg ml^{-1}). The stamp was then air-dried for 10 min at room temperature before printing fibronectin onto the microgrooved substrates. In the meantime, the µG surface was activated in UVO Cleaner for 7 min. The PDMS stamp was carefully placed onto the freshly cleaned microgrooved substrates for 30 s. Z-scan confocal microscopy (TCS SP5, Leica Microsystems, Wetzlar, Germany) was used to confirm the effectiveness of the fibronectin stamping.

2.2. Characterization of bio-adhesive and topographic patterned substrates

PDMS micropatterned and microgrooved replicas were characterized with an atomic force microscope (AFM; NanoWizard, JPK Instruments, Berlin, Germany). Images were acquired in contact mode using a silicon nitride tip with a nominal spring constant of approx. 0.1 N m^{-1} (MSCT, Bruker, Billerica, MA, USA). The scanning area was set at 50 × 50 µm, and images were recorded at a line-scan rate of 1 Hz in air at room temperature. At least three independent imaging scans were obtained for each sample. The mechanical properties of µP, µG and µG* patterned surfaces were measured using the same AFM but with a tip that has a nominal spring constant of approximately 0.6 N m^{-1} (MSCT). For the microgrooved surfaces, the AFM measurements were made on both the groove and ridge surfaces. Young's modulus (E) values were calculated from each force–displacement curve within a force map using the data analysis software JPKSPM Data Processing. The Hertz model was used to calculate Young's modulus for every force curve.

Contact angle (CA) measurements were performed to analyse wettability of all patterned and control substrates. In total, 50 µl of MilliQ water was dropped onto the substrates, and images for all tested conditions were acquired using a Photron Fastcam Mini UX100 camera with a 105 mm objective. For every water drop, five images were recorded and analysed with Fiji software [27].

2.3. Cell culture

Bovine aortic ECs (BAECs; Cell Applications, San Diego, CA, USA) in passages four to eight were cultured in complete Bovine Endothelial Cell Growth Medium (Cell Applications) at 37°C in a humidified atmosphere of 95% air and 5% CO_2; the culture medium was changed every 2 days. After 3 days of culture, cells were detached with trypsin (Gibco, Thermo Fisher Scientific, Waltham, MA, USA) and seeded on all patterned and control substrates at a density of 2×10^3 cells cm^{-2}. Prior to cell seeding, all patterned and control substrates were incubated for 1 h with 50 µg ml^{-1} fibronectin solution (Sigma-Aldrich, St. Louis, MO, USA) at room temperature.

2.4. Immunofluorescence

Cells cultured on all patterned and control substrates were fixed at 2 and 24 h after seeding with 4% paraformaldehyde (Alfa Aesar-Thermo Fisher, Karlsruhe, Germany) in PBS for 15 min. The cells were then permeabilized with 0.1% Triton X-100 (Sigma Aldrich-Merck KGaA, Darmstadt, Germany) in 1× PBS (TPBS). Samples were blocked in 3% bovine serum albumin in PBS (Sigma-Aldrich) for 1 h to avoid non-specific binding. FAs were labelled by incubating samples with an anti-vinculin monoclonal antibody (dilution 1 : 800, Sigma-Aldrich) for 1 h at 20°C. After incubation, substrates were washed three times with TPBS (3 min per wash) and incubated with Alexa Fluor 488-conjugated goat anti-mouse antibody (dilution 1 : 800; Jackson ImmunoResearch Inc., West Grove, PA, USA) for 1 h at 20°C. Actin filaments were stained by incubating samples with Alexa Fluor™ 594 or 633 phalloidin (dilution 1 : 250; ThermoFisher Scientific) for 1 h at 20°C. Samples were thoroughly rinsed in PBS and mounted on glass slides by using mounting media (Sigma-Aldrich). Fluorescent images of FAs and actin bundles were collected with a Leica TCS SP5 confocal microscope (Leica Microsystems). Samples were excited at 488 nm (vinculin) and 640 (actin), and the emissions were collected in the 500–530 nm and 660–690 nm ranges, respectively. Epifluorescent images were acquired using a Ti-U Eclipse inverted microscope (Nikon, Tokyo, Japan) which was equipped with an Orca Flash 4.0 camera (Hamamatsu, Shizuoka, Japan).

2.5. Image analysis

To assess cell elongation and orientation, epifluorescent images of TRITC phalloidin-stained cells were analysed with the MomentMacroJ v.1.3 script (hopkinsmedicine.org/fae/mmacro.htm) run in Fiji. Briefly, the macro calculates the second moment of area of grey scale images. For our purposes, we evaluated the principal moments of inertia (i.e. maximum and minimum), and we defined the cell elongation index (E.I.) as the ratio of the principal moments (maximum/minimum). Cell orientation was defined as the angle that the principal axis of inertia formed with a reference axis defined as the pattern direction for patterned substrates and the horizontal axis for control substrates.

Morphometric analysis (area, length and orientation) of FAs was performed in Fiji. Confocal digital images of FAs were first processed using the 'blur' command by following a modified version of the procedure proposed by Maruoka *et al.* [28]. Blurred images were subtracted from the original images using the image calculator command. The images were further processed with the 'threshold' command to obtain binary images. Pixel noise was eliminated using the 'erode' command and then particle analysis was performed in order to extract the morphometric descriptors. Only FAs whose area was above 0.5 μm^2 were included in the statistical analysis. Vinculin fluorescence intensity distribution on the different substrates was calculated using Fiji software.

2.6. Statistical analysis

Experiments were performed twice or three times at different time points. All data were expressed as mean ± s.e.m. Statistical comparison of EC morphology and FA features obtained on all patterned and control substrates were performed by ANOVA followed by the Tukey post-hoc analysis. A p-value < 0.05 was considered statistically significant. Statistical analysis on Young's modulus distributions was performed with the Kruskal–Wallis test in Matlab.

3. Results and discussion

3.1. Bio-adhesive and topographic patterned surfaces have similar effects on cellular alignment but not on cellular elongation

Previous studies have demonstrated that EC orientation is strongly responsive to substrate gratings, particularly in the 1–5 µm range. For instance, EC alignment is significantly enhanced when cells are cultured on microtopographies with 4–5 µm wide ridges/grooves and groove depths of 1–5 µm [29,30]. Here, we wish to specifically determine whether ECs respond similarly to planar versus topographic substrates with identical dimensions; thus, the scientific question of interest is whether the three-dimensional nature of a topographic patterned substrate *per se* leads to a different cytoskeletal organization (and by extension cellular elongation and alignment) from that induced by a two-dimensional (planar) substrate with the same pattern dimensions. In the light of the observations cited above on the effect of pattern dimensions on EC alignment [29,30], we opted for µP substrates consisting of 5 µm wide adhesive stripes separated by 5 µm wide PLL-PEG non-adhesive stripes and µG substrates possessing 5 µm wide ridge/groove micrograted surfaces with a groove depth of 1 µm. These dimensions ensured that the cells interacted with the grooves of the µG substrates and thus were able to sample the entire adhesive surface area available.

We used atomic force microscopy to verify the fidelity of the micropatterning and replica moulding processes. The measurements on µP surfaces demonstrated that deep UV irradiation of PEG-coated PDMS surfaces using the appropriate chrome mask was indeed effective in producing 5 µm wide PEG anti-adhesive stripes alternating with 5 µm wide non-functionalized stripes (figure 1*a*). The measurements also revealed a height difference between fibronectin and PLL-PEG stripes of approximately 45 nm. Since Franco *et al.* reported that a minimum groove depth of 0.6 µm is needed for ECs to exert contact guidance (in terms of elongation and alignment) [23], it is highly unlikely that ECs on our µP substrates were able to perceive a topographic effect due to the fibronectin molecular monolayer. For the microgrooved substrates, we measured groove and ridge widths of 5.6 ± 0.1 µm and 4.4 ± 0.1 µm, respectively, and a groove depth of 1 µm (figure 1*b*). Surface coating with fibronectin was used to promote EC-substrate adhesion. As expected, while fibronectin localized exclusively to the adhesive stripes of the µP surfaces (figure 1*c*), three-dimensional reconstruction of confocal images demonstrated that fibronectin was present on the surfaces of both the ridges and grooves of the µG substrates (figure 1*d*).

To elucidate the effect of bio-adhesive and topographic patterns on cell morphology and orientation, ECs were cultured on both the patterned surfaces and control substrates

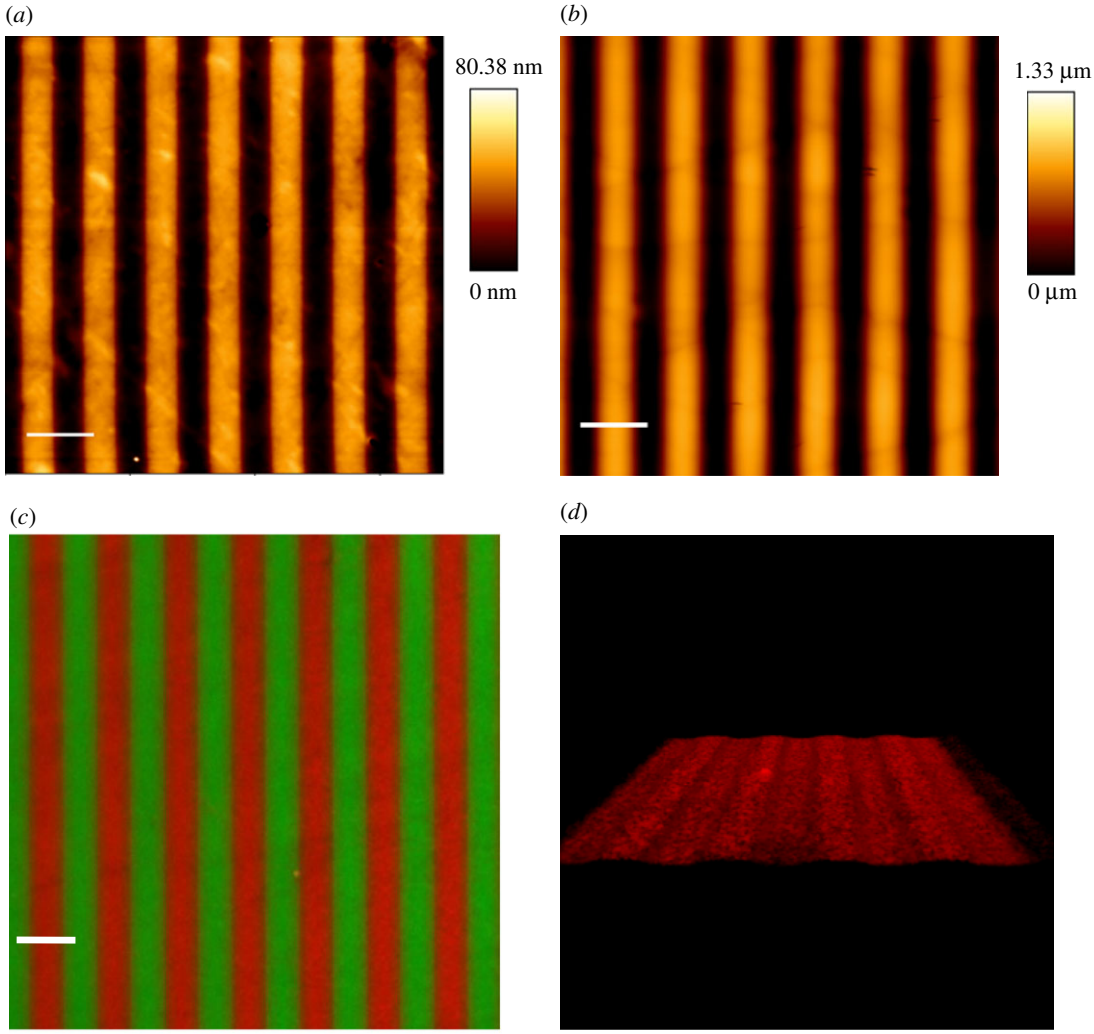

Figure 1. Bio-adhesive and topographic patterned surface characterization: atomic force microscopy images of (*a*) µP substrates and (*b*) µG substrates. The 5 µm wide dark stripes represent the adhesive stripes (*a*) and the groove surfaces (*b*), while the 5 µm wide orange stripes represent the PLL-PEG anti-adhesive areas (*a*, thickness 45 nm) and the ridge surfaces (*b*, depth = 1 µm). Scale bar is 10 µm. (*c*) Epifluorescent images of FITC-PLL-PEG (green) and rhodamine-fibronectin (red) coated µP surfaces. Scale bar is 10 µm. (*d*) Three-dimensional reconstruction of *z*-scanning confocal microscopy images of µG surface coated with rhodamine-fibronectin (red). (Online version in colour.)

for both short (2 h) and long (24 h) time periods. Figure 2*a–f* depicts representative confocal microscopy images of ECs on the various surfaces, and it shows marked differences between ECs seeded on patterned and unpatterned (control) substrates. More specifically, ECs on unpatterned substrates assumed a polygonal shape with thick and randomly oriented actin stress fibres at both 2 and 24 h after seeding. Conversely, ECs cultured on µP substrates possessed a spindle-like morphology with bundles of stress fibres well aligned in the pattern direction. On µG surfaces, ECs displayed morphologies that were intermediate between the µP and unpatterned cases.

To quantify how substrate patterning affected EC orientation, we first determined the angle between the cell major axis and either the pattern direction (for patterned surfaces) or the horizontal axis for unpatterned surfaces (figure 2*g*). ECs had an average angle of 43.0 ± 3.1° on unpatterned surfaces, consistent with randomly oriented cells as expected. Conversely, the bio-adhesive and topographic patterns provided a clear directional cue for cell alignment with the cell polarization axis at 2 h after seeding forming an angle relative to the pattern direction of 6.9 ± 0.8° and 9.3 ± 1.7° for the µP and µG substrates, respectively. The orientation did not change significantly at longer culture times, suggesting that EC alignment in the direction of the pattern develops rapidly.

Unlike their effect on cellular alignment, bio-adhesive and topographic patterned surfaces modulated EC morphology very differently (figure 2*h*). µP surfaces promoted marked cellular elongation, as quantified by the ratio of the principal moments of area of the cells, even after only 2 h of seeding (E.I. = 22.3 ± 3.5). This value decreased slightly, but not significantly, 24 h after seeding (E.I. = 18.9 ± 3.1), suggesting that µP substrates provided a rapid and efficient signal for cellular elongation. Conversely, ECs seeded on µG substrates exhibited a rather polygonal shape with E.I. values that were not statistically different from those observed on control unpatterned surfaces (E.I. = 5.8 ± 0.4 and 3.7 ± 0.4, respectively; $p > 0.05$). These data indicate that while planar bio-adhesive and topographic patterned surfaces similarly induce EC alignment, they have markedly different effects on cellular elongation.

3.2. Surface wettability and stiffness do not drive pattern-induced EC elongation

Chemical and mechanical properties of the substrate deeply impact cellular adhesion and spreading [31]. To determine

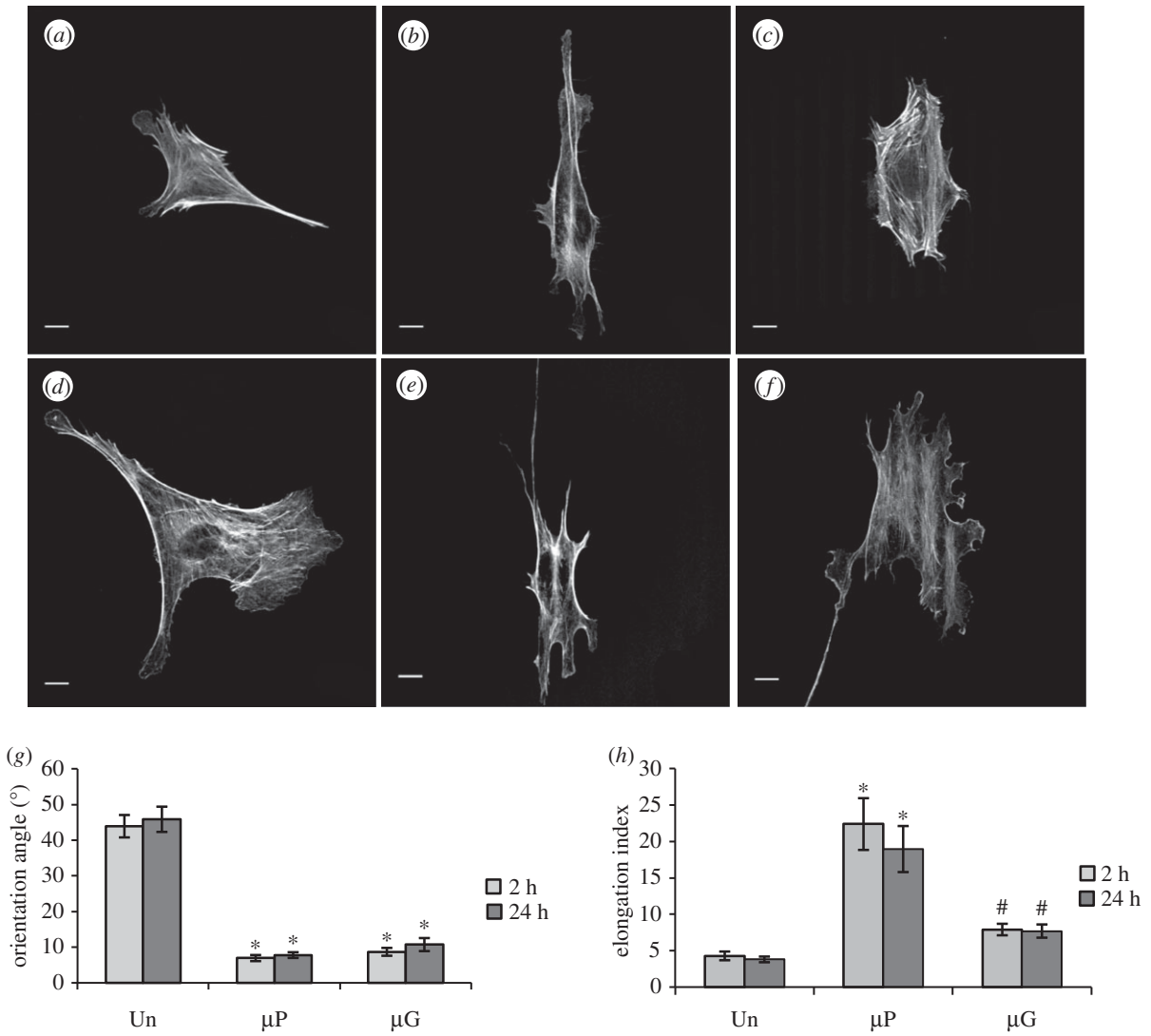

Figure 2. Bio-adhesive and topographic patterned surfaces have markedly different effects on cellular elongation: actin cytoskeleton confocal images of BAECs cultured on unpatterned control (*a*,*d*), µP (*b*,*e*) and µG (*c*,*f*) surfaces for 2 h (*a*–*c*) or 24 h (*d*–*f*). Scale bar is 10 µm. Cell orientation (*g*) and cell elongation index (h) of BAECs cultured on unpatterned ($n = 53$ cells), µP ($n = 52$ cells) and µG ($n = 49$ cells) surfaces from three independent experiments. Data are mean ± s.e.m. Asterisks (*) indicate statistically significant differences relative to the unpatented case, while hashtags (#) indicate statistically significant differences relative to the µP case ($p < 0.01$).

whether these properties synergized with surface patterning to drive the orientation and elongation of ECs, we first used water contact angle (CA) measurements to characterize the wettability of the µP and µG surfaces (electronic supplementary material, figure S1). The µG and unpatterned substrates were hydrophobic, with CA values of 92.0 ± 9.1° and 94.0 ± 8.9°, respectively (figure 3*a*). Chemical patterning (i.e. deep UV illumination) significantly reduced the hydrophobicity of the substrate, with the µP substrate exhibiting a CA of 68.5 ± 2.3°. We also measured the stiffness of the various substrates using an AFM. The measurements revealed that the µG and unpatterned substrates had significantly lower Young's modulus values (4.3 ± 0.9 MPa) than the µP substrates (31.8 ± 4.5 MPa). Since plasma surface treatment is required in order to graft PLL-PEG onto PDMS, we explored if the difference in surface wettability and substrate stiffness between the µP and µG substrates was attributable to this specific phase of the micropatterning process [32]. To this end, we produced microgrooved PDMS (µG*) and corresponding unpatterned control (Un*) substrates that had similar plasma/UV exposure to the µP substrate. FITC-PEG was employed in order to visualize the fluorescent signal before and after UV irradiation (electronic supplementary material, figure S2). As shown in figure 3*a*,*b*, the µG* and Un* substrates were more hydrophilic (CA values of 65.5 ± 7° and 52.6 ± 3°, respectively) and stiffer (Young's moduli of 37.1 ± 1.7 MPa and 47.3 ± 4.5 MPa, respectively) than their untreated counterparts. These results demonstrate that the µG* and Un* surfaces possessed comparable chemical and mechanical properties to those of the µP substrates.

We next tested the effect of the surface chemical and mechanical modifications induced by UV illumination on EC orientation and elongation. ECs cultured on Un* substrates were randomly oriented and had a similar E.I. to cells on control unpatterned surfaces (figure 3*c*,*d*). Furthermore, cellular orientation and elongation on the µG* substrate were comparable to those on the µG surface (figure 3*c*,*d*). These results suggest that the difference observed in cell elongation between ECs seeded on µP and µG surfaces (figure 2*h*) is not due to the chemical/mechanical surface properties but is rather attributable to other factors that drive the cellular elongation process.

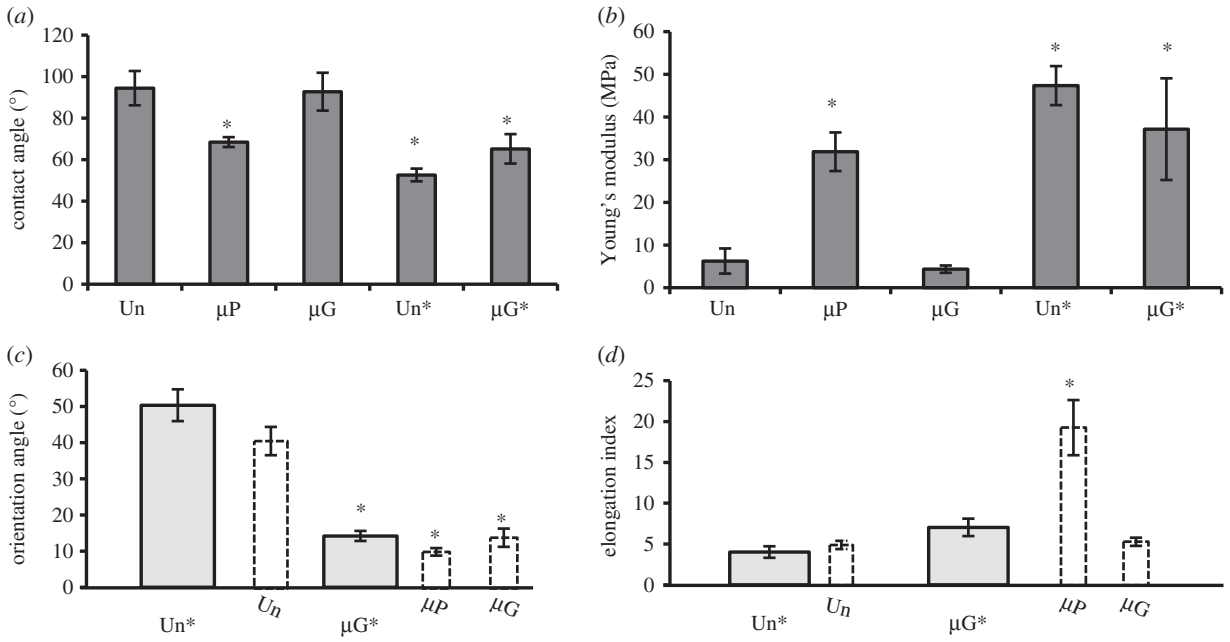

Figure 3. EC elongation on μP and μG surfaces is not due to the chemical/mechanical surface properties of the surfaces. (*a*) Water contact angle (CA) measurements on control and patterned substrates. Data are mean ± s.e.m. (*b*) AFM measurements of substrate stiffness for all control and patterned surfaces. Cell orientation (*c*) and cell elongation (*d*) of BAECs cultured on treated unpatterned surfaces (Un*, $n = 40$ cells) and treated microgrooved surfaces (μG*, $n = 81$ cells) from three independent experiments. The dashed bars (μP, μG and Unpatterned) are the 24 h data previously shown in figure 2 and presented again to facilitate the comparisons. Data are mean ± s.e.m. Asterisks (*) denote statistically significant differences relative to columns without asterisks ($p < 0.01$).

3.3. Bio-adhesive and topographic patterned surfaces have different effects on focal adhesion maturation and clustering

FAs are important regulators of cell-material crosstalk [33,34]. In fact, FA plaques constitute the mechanical link between the extracellular environment and the intracellular actin cytoskeleton with the adaptor protein vinculin enabling FA maturation and assuming a pivotal role in the maintenance of monolayer integrity [22–37]. We had previously demonstrated that topographic features in the form of nano- and micrograted adhesive surfaces provide a directional cue for the maturation of FAs in a specific direction, ultimately affecting cytoskeletal assembly and global cellular orientation [13]. We hypothesized that differences in FA clustering and maturation may explain the observed differences in how ECs perceive the μP and μG patterned surfaces (cf. figure 2*h*). To test this hypothesis, we analysed specific geometric features of FAs at late culture times (24 h after seeding) on all patterned and control surfaces. Confocal images of vinculin-labelled ECs revealed marked morphological differences between FAs on the planar bio-adhesive surfaces and those on the topographic patterned surfaces (figure 4). More specifically, ECs cultured on μP substrates formed significantly larger and longer FAs than on either μG or control substrates (figure 4*a*,*b*). While FAs were randomly oriented (average angle of 40.6 ± 0.7°) on control substrates, they were significantly more aligned in the direction of the pattern on both the μP and μG substrates (average angles of 20.1 ± 0.7° and 29.7 ± 0.9°, respectively; $p < 0.05$; figure 4*c*). These data demonstrate that although the fibronectin stripes on μP and microgrooved patterned surfaces are sufficiently wide (5 μm) to not exert significant confinement effects on FAs, they do orient FAs and guide their growth in a specific direction.

We also analysed the spatial distribution of FAs on the patterned and control substrates in order to elucidate the potential effect of planar bio-adhesive and topographic patterning on FA clustering. As expected, no particular FA distribution was observed on unpatterned substrates (figure 4*d*). When ECs were cultured on μP substrates, most of the mature FAs localized to the boundaries between the adhesive and non-adhesive zones (figure 4*e*). Conversely, FAs on μG substrates displayed a more heterogeneous distribution with localization both at the edges of the ridges and in the central regions of the grooves (figure 4*f*).

To further characterize the spatial assembly of FAs, we performed three-dimensional reconstruction of confocal images of the grooves and ridges of μG patterned surfaces. Although the majority of FAs were present on the ridges, FAs on the groove surfaces were larger, longer and highly aligned in the pattern direction (figure 5*a–c*). Thus, although the 5 μm width of the grooves was sufficiently large to not confer significant physical confinement on FAs, the grooves appear to play an important role in promoting FA anisotropic maturation. The cell membrane suspended on the ridge top can thus deform sufficiently to make contact with the groove surface. As in a 3-point bending test of an elastic shell, the most efficient mode of deformation is by applying a force half way down the shell span; thus, it may be that anchoring the cell membrane at the groove centre would cause a membrane tension sufficiently low to be resisted by FAs. In fact, the longest FAs on the groove surface were observed near the centre of the groove. Deviations from this condition would require the cell membrane to display a much higher curvature, hence exerting higher tensions. The presence of the ridge edges reduced but did not abolish the possibility of ECs to 'climb up' the ridge walls and form FAs on the ridge surface. Altogether these data show that

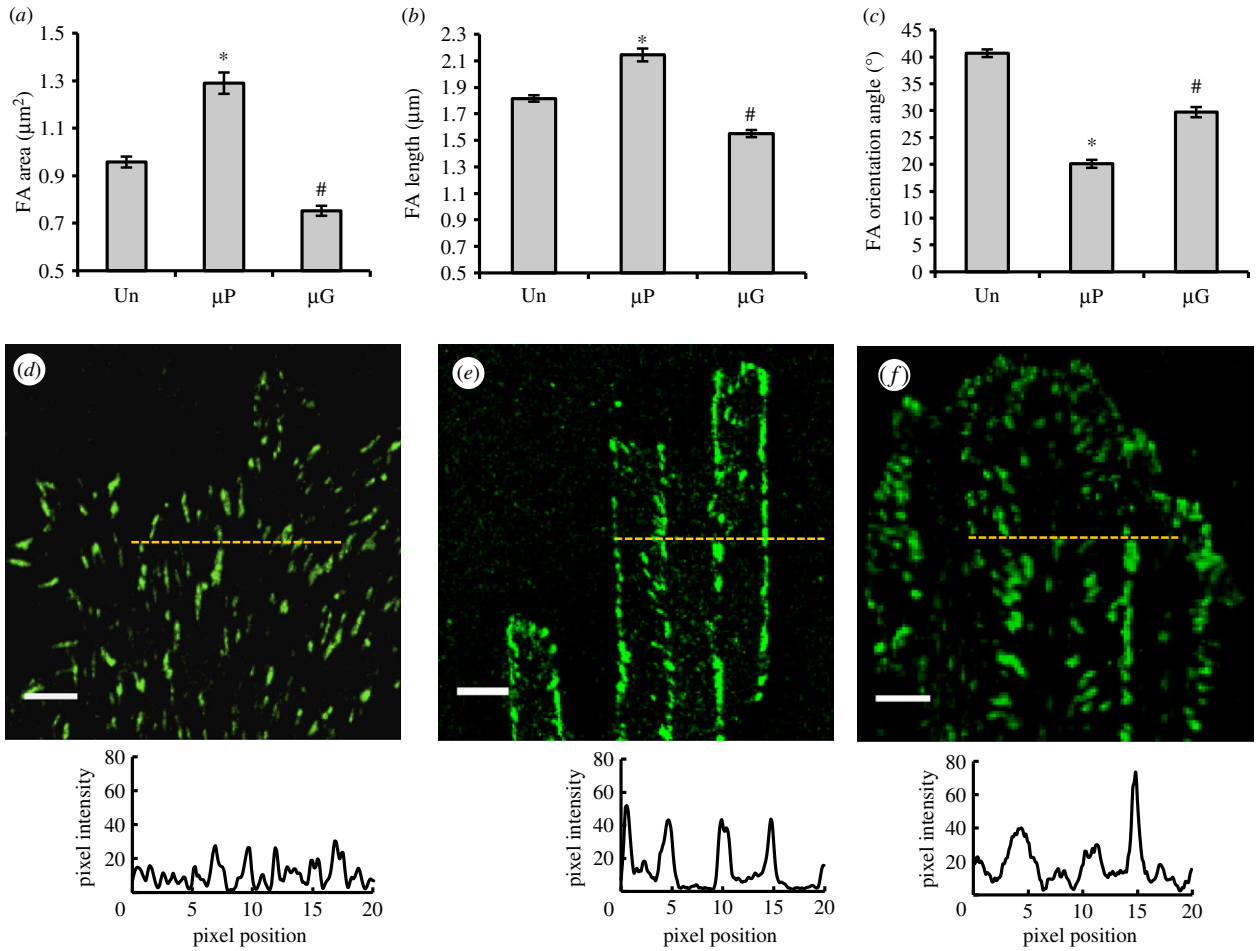

Figure 4. Focal adhesion (FA) maturation on control and patterned surfaces: FA area (*a*), length (*b*) and orientation (*c*) of BAECs cultured for 24 h on pattered and control surfaces. 1296, 876 and 668 FAs from three independent experiments were measured on unpatterned, μP and μG substrates, respectively. Data are mean ± s.e.m. Asterisks (*) indicate statistically significant differences relative to the corresponding Un case ($p < 0.01$), while hashtags (#) denote statistically significant differences relative to both the Un and μP cases ($p < 0.01$). Confocal images of vinculin (green) and corresponding fluorescence intensity distribution profiles of BAECs cultured for 24 h on unpatterned (*d*), μP (*e*) and μG (*f*) substrates. The zero position corresponds to the beginning of an adhesive stripe for the planar bio-adhesive patterned surface and the beginning of a ridge for the microgrooved patterned surface. Scale bar is 5 μm. (Online version in colour.)

the presence of the microgroove side walls promotes the maturation of FAs in the central region of the groove and guides their growth preferentially along the pattern direction (figure 5*d*). By contrast, FAs on the ridges have sufficient space to mature and to orient in a wider range of directions.

In order to determine whether the geometric features of the topographic pattern enabled sufficient membrane deformation to allow FA formation on the groove surface, we cultured ECs on μG-2 μm (with groove depth of 1 μm) and μG-0.7 μm (groove depth of 0.25 μm) surfaces. In these cases, FAs were only visible on the ridges (electronic supplementary material, figure S3), suggesting that the 5 μm width of the topographic features of the μG surface was sufficiently large to allow FA access to the groove surface but that significantly narrower ridges preclude such access. Based on these findings, we propose that the interactions occurring inside the groove are responsible for the formation of aligned FAs, providing a powerful stimulus for the alignment of ECs along the microgroove direction.

3.4. Adhesive protein distribution drives cellular elongation

The evidence reported so far suggests that the 5 μm wide and 1 μm deep grooves enable the formation of long and aligned FAs that further stabilize EC elongation and orientation along the pattern direction. However, why ECs on μG substrates are significantly less elongated than on μP surfaces (cf. figure 2*h*) is still unclear. As already shown (cf. figure 1*d*), fibronectin adsorbed to the entire μG surface, with the fluorescent signal detected on both the ridges and the grooves. Thus, on μG substrates the surface area available for the establishment of mature FAs was approximately twice that of μP substrates in which PLL-PEG lines prevented the formation of FAs. We used micro-contact printing to fabricate a three-dimensional topographic pattern with an adhesive area comparable to that of μP substrates, termed μG-FnR, where fibronectin was selectively adsorbed on the ridge (but not the groove) as confirmed by three-dimensional reconstruction of confocal microscopy images (electronic supplementary material, figure S4). ECs cultured on μG-FnR substrates were more aligned along the pattern direction (angle of 3.8 ± 0.5°) than those on either μP or μG surfaces (figure 6*b*). Importantly, ECs on μG-FnR substrates were even more elongated than those on μP surfaces (figure 6*c*).

Because the μG-FnR substrate was effective in elongating ECs and since FAs on the μP substrate clustered at the boundaries between the adhesive and non-adhesive zones, we hypothesized that FAs on the μG-FnR surface preferentially

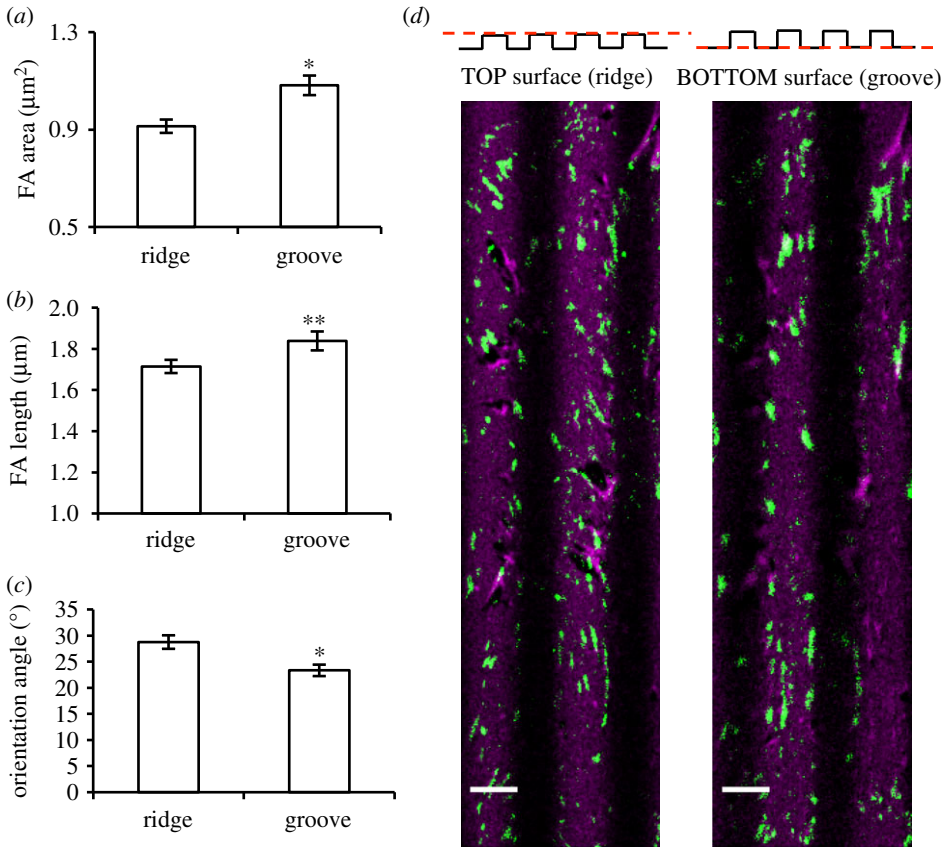

Figure 5. Ridge and groove affect focal adhesion (FA) maturation differently: FA area (*a*), length (*b*) and orientation (*c*) of BAECs cultured for 24 h on μG surfaces. Results are shown separately for FAs forming on the ridge ($n = 467$) and groove ($n = 504$) surfaces. Data are mean ± s.e.m. Asterisks denote statistically significant differences from ridges (*$p < 0.01$, **$p < 0.05$). (*d*) Representative *z*-scan confocal images of FAs (vinculin, green) and fibronectin (magenta) on the ridge and groove surfaces of the μG substrate. Scale bar is 5 μm. (Online version in colour.)

localize to the edges of the ridges. To test this hypothesis, we analysed confocal microscopy images and confirmed that FAs formed only on the ridges but not in the grooves (figure 6*a*). Moreover, we observed that ECs formed longer and larger FAs on the μG-FnR substrates than on the μG substrates, with average values not statistically different from those on μP substrates (figure 6*d*,*e*). Abolishing FA formation in the grooves resulted in FAs on the ridges that were even more aligned along the pattern direction (15.1 ± 0.6°) than those in all other tested conditions (figure 6*f*). These findings strongly suggest that the FA clustering that occurs with alternating adhesive and non-adhesive zones of appropriate dimensions promotes EC elongation along a particular direction. In support of this notion, a similar FA organization was observed when ECs were cultured on μG-2 μm substrates and the resulting elongation index was not significantly different from that observed on the μG-FnR surfaces (28.0 ± 7.7 versus 33.3 ± 3.7; $p > 0.05$; electronic supplementary material, figure S5). These results suggest that once the cellular interaction with the groove surface is abrogated by engineering the adhesive properties of topographic patterned surfaces, the maturation of FAs is tuned to accommodate the areas available for cell adhesion and FA formation. Finally, FAs on the μG-FnR surfaces localized preferentially along the edges of the adhesive ridges (figure 6*g*), thus confirming our hypothesis that EC morphology and orientation are driven by the localization and clustering of FAs. To recapitulate, table 1 provides a general summary of the findings of the effects of the various surfaces on EC elongation and alignment.

3.5. Bio-adhesive and topographic patterned surfaces impact stress fibre assembly differently

The actin cytoskeleton is a critical regulator of EC function. A particularly interesting observation is that actin stress fibre alignment has a protective effect on ECs challenged with a pro-inflammatory stimulus even in the absence of external fluid shear stress [9]. Since FAs act to organize actin stress fibres in cells, we expect that the observed differences in FA size and clustering between planar bio-adhesive and topographic patterned substrates would lead to differences in stress fibre assembly and organization. We used confocal microscopy to visualize the spatial distribution of actin filaments in ECs cultured on all the different surfaces. In ECs cultured on unpatterned substrates, stress fibres exhibited a random spatial orientation with dense peripheral actin microfilament bundles (cf. figure 2*a*,*d*), typical of ECs cultured under static (no flow) conditions [38]. As shown in figure 7*a*, μP substrates provided guidance for the assembly of the actin network. More specifically, along the EC basal plane, we observed bundles of actin fibres running parallel to the pattern direction over a large portion of the cell body. These actin bundles were always detected in between adjacent fibronectin stripes, bridging FAs located at the borders of neighbouring adhesive areas. Additionally, in most of the cases, the leading edge of the EC body protruded in the direction of the pattern, with well-defined cortical actin perfectly retracing the contour of the adhesive stripes. On the other hand, when ECs were cultured on μG surfaces, confocal *z*-stack imaging revealed the existence of two families of

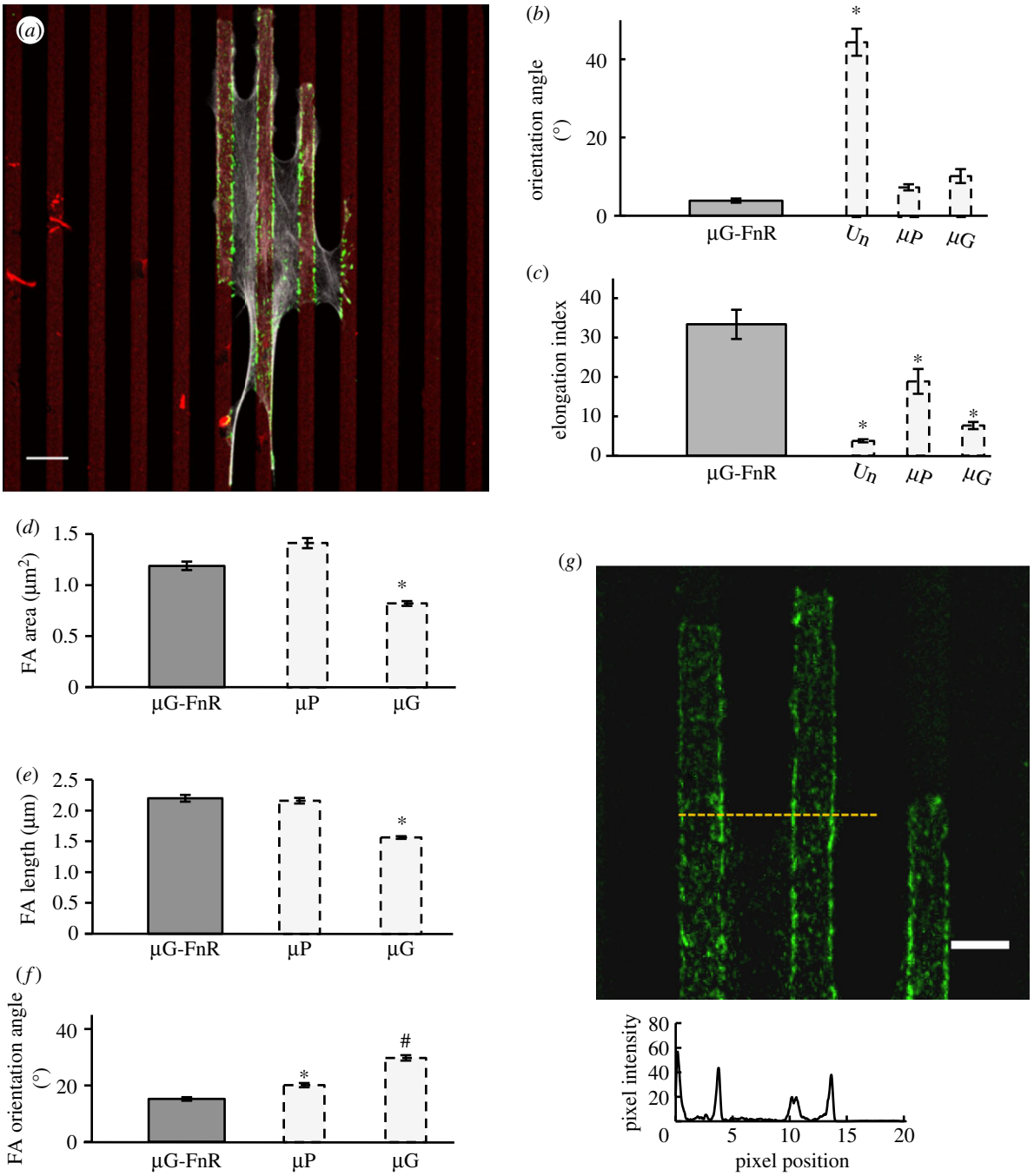

Figure 6. μG-FnR surfaces promote cellular elongation. (*a*) Confocal image of a BAEC cultured for 24 h on the μG-FnR substrate. FA (green), actin stress fibres (grey) and adhesive areas (red) are visualized with anti-vinculin antibody, phalloidin and rhodamine-fibronectin, respectively. Scale bar is 10 μm. Cell orientation (*b*) and cell elongation index (*c*) from three independent experiments on BAECs cultured for 24 h on μG-FnR surfaces ($n = 45$ cells). The dashed bars (unpatterned, μP and μG) are the 24 h data previously shown in figure 2 and presented again to facilitate the comparisons. FA area (*d*), length (*e*) and orientation (*f*) of BAECs cultured for 24 h on μG-FnR substrates. Data are from three independent experiments. The dashed bars (μP, μG) are the data previously shown in figure 4 and presented again to facilitate the comparisons. All data are mean ± s.e.m. Asterisks denote statistically significant differences relative to the corresponding unmarked bars, while hashtags denote statistically significant differences relative to both unmarked bars and bars marked with asterisks $^{*}p < 0.01$, $^{\#}p < 0.05$). (*g*) Representative confocal image of vinculin (green) and corresponding fluorescence intensity distribution profile for BAECs cultured for 24 h on the μG-FnR substrate. The zero position corresponds to the beginning of a ridge. Scale bar is 5 μm. (Online version in colour.)

stress fibres possessing different spatial arrangements: stress fibres on the ridges did not exhibit any clear spatial organization, whereas stress fibres inside the grooves formed highly packed bundles oriented in the pattern direction (figure 7*b*,*c*). These bundles were associated with the long and well-aligned FAs detected inside the groove, suggesting that the groove surface provided a potent directional guidance for the maturation and spatial organization of stress fibres. When ECs were cultured on μG-FnR surfaces in which the groove was no longer accessible for adhesion, the actin network arrangement had several similarities to that observed in cells on μP substrates, most notably the presence between adjacent adhesive ridges of suspended thick stress fibre bundles running along the cell body (figure 7*d*). These bundles connected FAs located at the boundaries of neighbouring adhesive ridges and thus presumably formed suspended bridges between adjacent ridges.

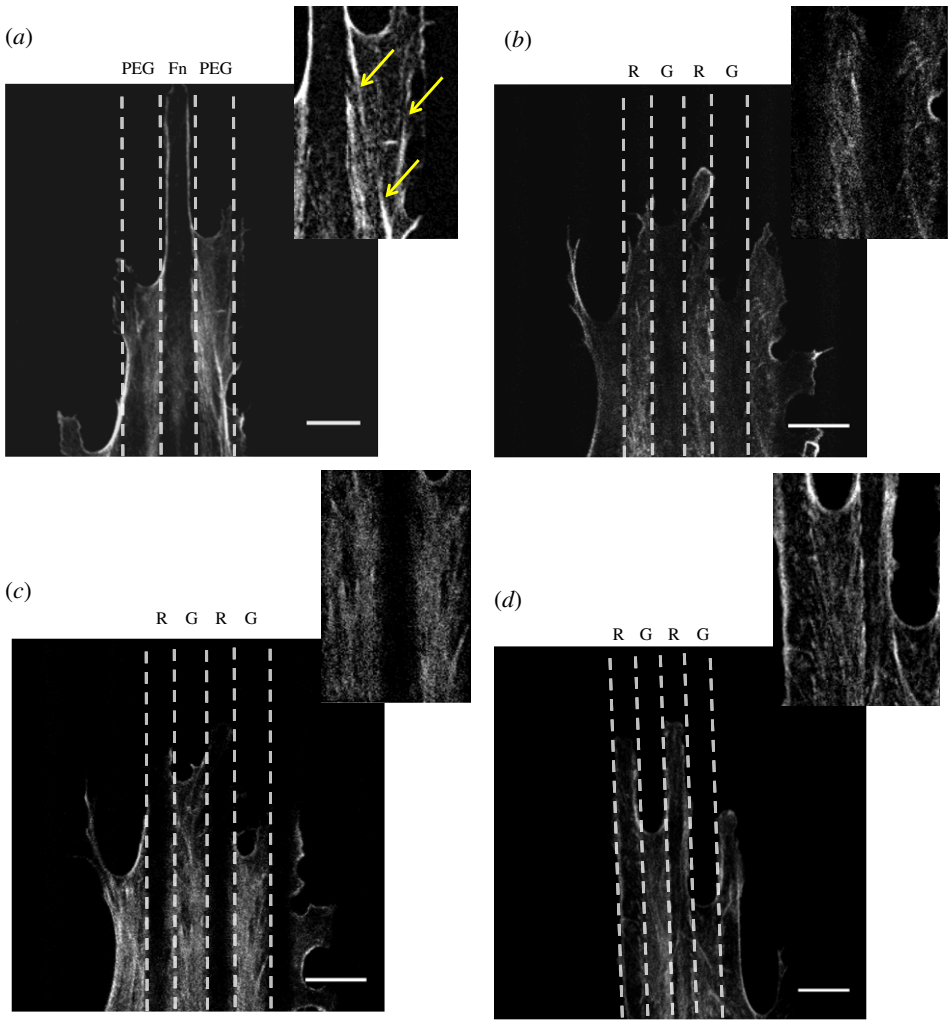

Figure 7. Planar bio-adhesive and topographic patterned substrates affect stress fibre assembly differently. Actin cytoskeleton confocal images of BAECs cultured for 24 h on μP (*a*), μG ridge (*b*), groove (*c*) and μG-FnR (*d*) surfaces. The dashed lines define the adhesive (fibronectin)/non-adhesive (PLL-PEG) areas of the μP surface and the topographic ridge/groove (R/G) features of the μG-FnR and μG surfaces. Scale bar is 5 μm. Insets provide zoom-in views of stress fibres. Yellow narrows indicate aligned actin bundles on μP surfaces. (Online version in colour.)

Table 1. Effects of patterned surfaces on EC alignment and elongation.

	alignment	elongation
μP	yes	yes
μG	yes	no
μG*	yes	no
μG-FnR	yes	yes
μG_2 μm	yes	yes

A question arises as to how the interplay between FA clustering and stress fibre assembly promotes cellular elongation. One possibility is that the structural reinforcement provided by contractile stress fibre cables that run laterally over the non-adhesive stripes reduces the capacity of ECs to extend orthogonal to the pattern direction. Théry *et al.* suggested that stress fibre cable reinforcement over non-adhesive zones is directly due to the transmission of membrane tension to the stress fibres while the attachments along the adhesive edges may reduce the inward pulling of the membrane on the actin cables as well as provide local relays that reduce cable tension [39]. A second possibility resides in the dynamic nature of FAs, which can glide on surfaces under the effect of traction forces in a sort of tread-milling mechanism [40]. FAs lying on the very same ridge or stripe and connected to a stress fibre may eventually come close to each other and collapse. If FAs are separated by a non-conducive region such as grooves or cell-repellant stripes, the inhibition of movement of FAs in close proximity to the adhesive region edges resists stress fibre contraction, ultimately stabilizing FA–stress fibre assembly.

To further investigate whether the peculiar FA/stress fibre organization described above provides a stimulus for EC elongation in the direction of the pattern, we treated ECs with blebbistatin (10 mM for 24 h) which inhibits cell tail retraction and has been reported to induce dramatic elongation of the posterior region of the cell [41]. After treatment with blebbistatin, ECs cultured on unpatterned substrates assumed a dendritic-like morphology with particularly prominent F-actin staining along cell borders (figure 8*a*). Stress fibres could still be observed throughout the cytoplasm, suggesting that the concentration of blebbistatin used here did not completely abolish stress fibre formation. As expected, ECs remained randomly oriented but were more elongated relative to untreated cells (figure 8*e*). Surprisingly, for ECs on the μP and μG-FnR substrates, blebbistatin treatment had no effect on cell alignment or elongation (figure 8*b*,*d*–*f*). Even though narrow cellular

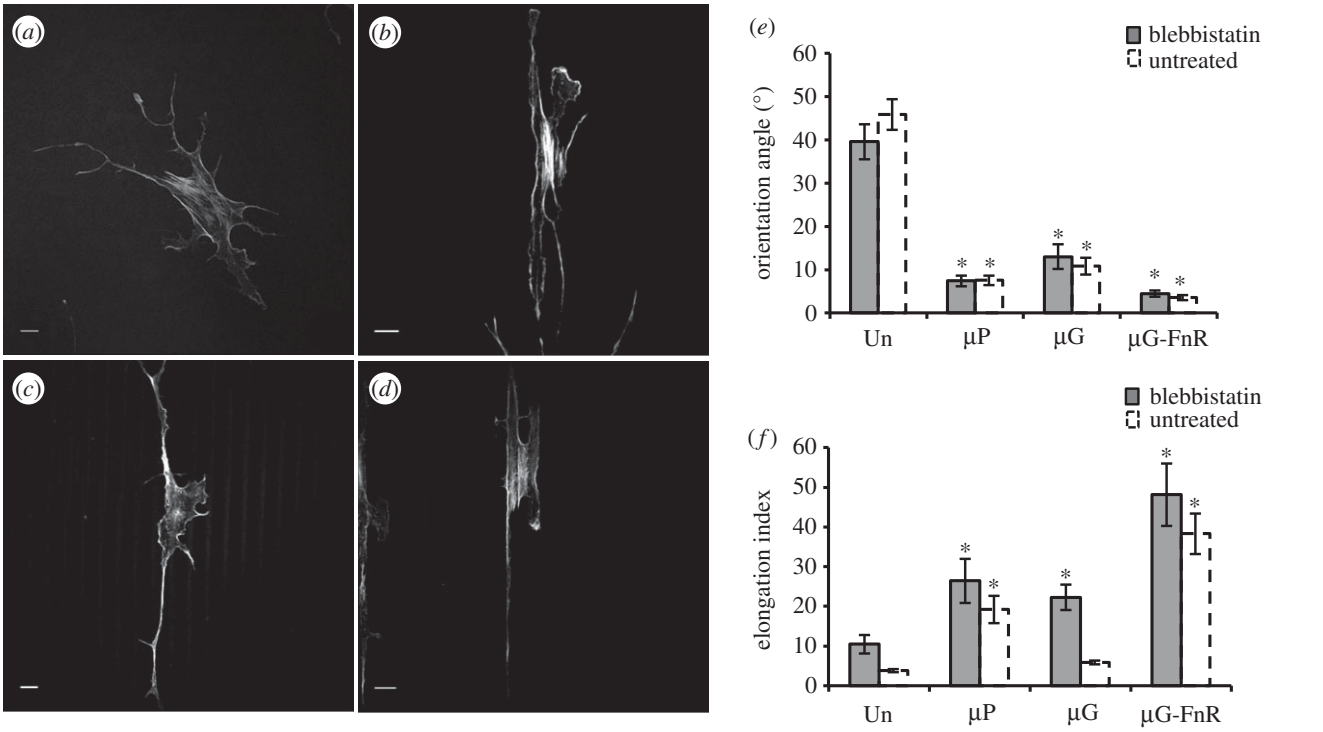

Figure 8. Actomyosin contractility is modulated differently by planar bio-adhesive and topographic patterned substrates: actin cytoskeleton confocal images of blebbistatin-treated (10 mM) BAECs cultured for 24 h on unpatterned control (*a*), µP (*b*), µG (*c*) and µG-FnR (*d*) surfaces. Scale bar is 10 µm. Cell orientation (*e*) and elongation index (*f*) of blebbistatin-treated BAECs (number of cells: Un = 42, µP = 45, µG = 42, µG-FnR = 38) from two independent experiments. Data are mean ± s.e.m. The dashed bars correspond to previously shown data from figures 2 and 6 (untreated cells) and presented again to facilitate the comparisons. Asterisks denote statistically significant differences relative to the unmarked bars (*$p < 0.01$).

processes appeared after blebbistatin treatment, a dense meshwork of well-aligned fibres was still present in the central part of the EC body. Interestingly, ECs on the µG substrates were particularly sensitive to blebbistatin treatment with a marked increase in cellular elongation following drug treatment (E.I. values of 22.2 ± 3.1 for blebbistatin-treated ECs versus 5.8 ± 0.4 for untreated cells; figure 8*c*,*f*). Furthermore, *z*-stack confocal imaging demonstrated that blebbistain treatment affected FAs on the ridges differently from those in the grooves. More specifically, even if small FAs were still present along the extreme cell periphery and associated with spikes and processes, mature FAs were mostly observed along the edges of the ridges and inside the grooves (electronic supplementary material, figure S6). Larger and well-aligned FAs associated with thick bundles of actin stress fibres were detected inside the groove, suggesting a role for surface recesses in preserving FAs and actin fibre network assembly.

4. Conclusion

In the present work, we explored how vascular ECs perceive planar bio-adhesive and topographic patterned surfaces, and we investigated the mechanisms by which patterned surfaces regulate cellular elongation and alignment. These two physical attributes have been shown to regulate immunogenic gene expression and function and may act synergistically with fluid shear stress to create an EC surface with reduced susceptibility to inflammation [9]. We found that while µP and µG patterned substrates are equally effective in inducing EC alignment, cellular elongation was considerably more prominent on the µP substrates. We also determined that the mechanism by which planar bio-adhesive and topographic patterned substrates modulate cellular morphology involves the effect of these substrates on FA clustering and subsequent cytoskeletal organization. More specifically, we found that on planar bio-adhesive surfaces, FA localization to the boundaries between the adhesive and non-adhesive zones drives ECs elongation along the pattern direction. On the other hand, on microgrooved topographic surfaces, the availability of the groove surface to FA formation plays a critical role in determining EC morphology, reducing the elongation with respect to bio-adhesive patterned surfaces. However, once the cellular interaction with the groove surface is abrogated by engineering the adhesive properties of the topographic patterned surface, FAs localize preferentially along the edges of the adhesive ridges and promote extensive EC elongation, thus confirming our hypothesis that EC morphology and orientation are driven by the localization and clustering of FAs. Changes in cell morphology and orientation might not be the only cellular characteristics affected by adhesion patterning through microprinting or surface topography. Complex biochemical pathways can also be affected and/or regulated by differences in the organization of FAs or cytoskeletal structures. In the case of endothelia, recent literature has highlighted the interplay between cytoskeletal components and the dynamics of the VEGF receptor VEGFR-2. Notably, inhibition of actin filaments causes signalling disruption of the ERK1/2 pathway [42]. Indeed, substrates that alter cytoskeletal maturation and arrangement profoundly affect VEGFR-2 internalization and hence ERK1/2 phosphorylation [43]. In the light of these associations, the notion that surface pattern designs may turn specific signalling pathways on or off certainly merits future investigation.

Finally, the present results provide novel insight into the effects of substrate biophysical cues on EC behaviour and

promise to inform strategies aimed at optimizing the performance of the surfaces of implantable cardiovascular devices. We speculate that embossing or printing-specific micropatterns on the luminal surface of an implanted endovascular device might coax ECs that ultimately cover the device to acquire an elongated and aligned morphology that may be associated with a cellular phenotype that is less susceptible to inflammation, thus improving the biocompatibility and potentially the patency of the device. In support of this notion, recent work has described a micropatterned coronary stent that appears to be associated with decreased neointimal hyperplasia in a porcine coronary injury model [25]. It should be emphasized, however, that the microfabrication technologies and chemical functionalization strategies need to be carefully optimized in order to ensure the long-term stability of adhesive patterns in the complex *in vivo* environment.

Data accessibility. The datasets supporting this article have been uploaded as part of the electronic supplementary material.

Authors' contributions. C.F.N., J.J.L. and A.I.B. designed the study. C.F.N. performed the experimental work and analyses. M.V. contributed to characterization of the substrate mechanical properties. A.B. provided technical assistance for the experiments. C.F.N., J.J.L., M.V., A.B. and A.I.B. contributed technical support and discussion. C.F.N., J.J.L., M.V. and A.I.B. wrote/edited the manuscript.

Competing interests. We declare we have no competing interests.

Funding. This work was supported by a research grant from the Fondation Lefoulon-Dellalande and an endowment in cardiovascular bioengineering from the AXA Research Fund. The confocal microscope was acquired in part through the support of the Agence Nationale de la Recherche (contract ANR-10-ANR-11-EQPX-0029 Morphoscope2).

Acknowledgements. The authors thank Pierre Lecointre, Pierre Mahou and Valeria Panzetta for providing help in contact angle characterization, confocal image acquisition and AFM measurements, respectively.

References

1. Chen CS, Mrksich M, Huang S, Whitesides GM, Ingber DE. 1997 Geometric control of cell life and death. *Science* **276**, 1425–1428. (doi:10.1126/science.276.5317.1425)
2. Shah JV. 2010 Cells in tight spaces: the role of cell shape in cell function. *J. Cell Biol.* **191**, 233–236. (doi:10.1083/jcb.201009048)
3. Vogel V, Sheetz MJ. 2006 Local force and geometry sensing regulate cell functions. *Nat. Rev. Mol. Cell Biol.* **7**, 265–275. (doi:10.1038/nrm1890)
4. Berk BC, Abe JI, Min W, Surapisitchat J, Yan C. 2001 Endothelial atheroprotective and anti-inflammatory mechanisms. *Ann. N Y Acad. Sci.* **947**, 93–109. (doi:10.1111/j.1749-6632.2001.tb03932.x)
5. Hahn C, Schwartz MA. 2009 Mechanotransduction in vascular physiology and atherogenesis. *Nat. Rev. Mol. Cell Biol.* **10**, 53–62. (doi:10.1038/nrm2596)
6. Davies PF, Remuzzi A, Gordon EJ, Dewey CF, Gimbrone Jr MA. 1986 Turbulent fluid shear stress induces vascular endothelial cell turnover *in vitro*. *Proc. Natl. Acad. Sci. USA.* **83**, 2114–2117.
7. Kim DW, Gotlieb AI, Langille BL. 1989 In vivo modulation of endothelial F-actin microfilaments by experimental alterations in shear stress. *Arteriosclerosis* **9**, 439–445. (doi:10.1161/01.atv.9.4.439)
8. Chien S. 2008 Effects of disturbed flow on endothelial cells. *Ann. Biomed. Eng.* **36**, 554–562. (doi:10.1007/s10439-007-9426-3)
9. Vartanian KB, Berny MA, McCarty OJ, Hanson SR, Hinds MT. 2010 Cytoskeletal structure regulates endothelial cell immunogenicity independent of fluid shear stress. *Am. J. Physiol. Cell Physiol.* **298**, C333–C341. (doi:10.1152/ajpcell.00340.2009)
10. Roca-Cusachs P, Alcaraz J, Sunyer R, Samitier J, Farré R, Navajas D. 2008 Micropatterning of single endothelial cell shape reveals a tight coupling between nuclear volume in G1 and proliferation. *Biophys. J.* **94**, 4984–4995. (doi:10.1529/biophysj.107.116863)
11. Versaevel M, Grevesse T, Gabriele S. 2012 Spatial coordination between cell and nuclear shape within micropatterned endothelial cells. *Nat. Commun.* **3**, 671. (doi:10.1038/ncomms1668)
12. Flemming RG, Murphy CJ, Abrams GA, Goodman SL, Nealey PF. 1999 Effects of synthetic micro- and nano-structured surfaces on cell behavior. *Biomaterials* **20**, 573–588. (doi:10.1016/s0142-9612(98)00209-9)
13. Natale CF, Ventre M, Netti PA. 2014 Tuning the material-cytoskeleton crosstalk via nanoconfinement of focal adhesions. *Biomaterials* **35**, 2743–2751. (doi:10.1016/j.biomaterials.2013.12.023)
14. Liliensiek SJ, Wood JA, Yong J, Auerbach R, Nealey PF, Murphy CJ. 2010 Modulation of human vascular endothelial cell behaviors by nanotopographic cues. *Biomaterials* **31**, 5418–5426. (doi:10.1016/j.biomaterials.2010.03.045)
15. Ray A, Lee O, Win Z, Edwards RM, Alford PW, Kim DH, Provenzano PP. 2017 Anisotropic forces from spatially constrained focal adhesions mediate contact guidance directed cell migration. *Nat. Commun.* **8**, 14923. (doi:10.1038/ncomms14923)
16. Brody S, Anilkumar T, Liliensiek S, Last JA, Murphy CJ, Pandit A. 2006 Characterizing nanoscale topography of the aortic heart valve basement membrane for tissue engineering heart valve scaffold design. *Tissue Eng.* **12**, 413–421. (doi:10.1089/ten.2006.12.413)
17. Liliensiek SJ, Nealey P, Murphy CJ. 2009 Characterization of endothelial basement membrane nanotopography in rhesus macaque as a guide for vessel tissue engineering. *Tissue Eng. Part A* **15**, 2643–2651. (doi:10.1089/ten.TEA.2008.0284)
18. Chung TW, Liu DZ, Wang SY, Wang SS. 2003 Enhancement of the growth of human endothelial cells by surface roughness at nanometer scale. *Biomaterials* **24**, 4655–4661. (doi:10.1016/S0142-9612(03)00)
19. Biela SA, Su Y, Spatz JP, Kemkemer R. 2009 different sensitivity of human endothelial cells, smooth muscle cells and fibroblasts to topography in the nano-micro range. *Acta Biomater.* **5**, 2460–2466. (doi:10.1016/j.actbio.2009.04.003)
20. Morgan JT, Wood JA, Shah NM, Hughbanks ML, Russell P, Barakat AI, Murphy CJ. 2012 Integration of basal topographic cues and apical shear stress in vascular endothelial cells. *Biomaterials* **33**, 4126–4135. (doi:10.1016/j.biomaterials.2012.02.047)
21. Anderson DE, Hinds MT. 2011 Endothelial cell micropatterning: methods, effects, and applications. *Ann. Biomed. Eng.* **39**, 2329–2345. (doi:10.1007/s10439-011-0352-z)
22. Kanchanawong P, Shtengel G, Pasapera AM, Ramko EB, Davidson MW, Hess HF, Waterman CM. 2010 Nanoscale architecture of integrin-based cell adhesions. *Nature* **468**, 580–584. (doi:10.1038/nature09621)
23. Franco D, Klingauf M, Bednarzik M, Cecchini M, Kurtcuoglu V, Gobrecht J, Poulikakosa D, Ferrari A. 2011 Control of initial endothelial spreading by topographic activation of focal adhesion kinase. *Soft Matter* **7**, 7313–7324. (doi:10.1039/C1SM05191A)
24. Uttayarat P, Toworfe GK, Dietrich F, Lelkes PI, Composto RJ. 2005 Topographic guidance of endothelial cells on silicone surfaces with micro- to nanogrooves: orientation of actin filaments and focal adhesions. *J. Biomed. Mater. Res. A.* **75**, 668–680. (doi:10.1002/jbm.a.30478)
25. Sprague EA, Tio F, Ahmed SH, Granada JF, Bailey SR. 2012 Impact of parallel micro-engineered stent grooves on endothelial cell migration, proliferation, and function: an in vivo correlation study of the healing response in the coronary swine model. *Circ. Cardiovasc. Interv.* **5**, 499–507. (doi:10.1161/CIRCINTERVENTIONS.111.967901)
26. Azioune A, Carpi N, Tseng Q, Théry M, Piel M. 2010 Protein micropatterns: a direct printing protocol using deep UVs. *Methods Cell Biol.* **97**, 133–146. (doi:10.1016/S0091-679X(10)97008-8.)
27. Schindelin J, Arganda-Carreras I, Frise E. 2012 Fiji: an open-source platform for biological-image analysis. *Nat. Methods.* **9**, 676–682. (doi:10.1038/nmeth.2019)

28. Maruoka M, Sato M, Yuan Y, Ichiba M, Fujii R, Ogawa T, Ishida-Kitagawa N, Takeya T, Watanabe N. 2012 Abl-1-bridged tyrosine phosphorylation of VASP by abelson kinase impairs association of VASP to focal adhesions and regulates leukaemic cell adhesion. *Biochem. J.* **441**, 889–899. (doi:10.1042/BJ20110951)
29. Feinberg AW, Wilkerson WR, Seegert CA, Gibson AL, Hoipkemeier-Wilson L, Brennan AB. 2008 Systematic variation of microtopography, surface chemistry and elastic modulus and the state dependent effect on endothelial cell alignment. *J. Biomed. Mater. Res. A.* **86**, 522–534. (doi:10.1002/jbm.a.31626)
30. Uttayarat P, Chen M, Li M, Allen FD, Composto RJ, Lelkes PI. 2008 Microtopography and flow modulate the direction of endothelial cell migration. *Am. J. Physiol. Heart Circ. Physiol.* **294**, 1027–1035. (doi:10.1152/ajpheart.00816.2007)
31. Ventre M, Netti PA. 2016 Controlling cell functions and fate with surfaces and hydrogels: the role of material features in cell adhesion and signal transduction. *Gels* **2**, 12. (doi:10.3390/gels2010012)
32. Yang Y, Kulangara K, Lam RT, Dharmawan R, Leong KW. 2012 Effects of topographical and mechanical property alterations induced by oxygen plasma modification on stem cell behavior. *ACS Nano* **6**, 8591–8598. (doi:10.1021/nn301713d)
33. Diener A, Nebe B, Lüthen F, Becker P, Beck U, Neumann HG, Rychly J. 2005 Control of focal adhesion dynamics by material surface characteristics. *Biomaterials* **26**, 383–392. (doi:10.1016/j.biomaterials.2004.02.038)
34. Wozniak MA, Modzelewska K, Kwong L, Keely PJ. 2004 Focal adhesion regulation of cell behavior. *Biochim. Biophys. Acta.* **1692**, 103–119. (doi:10.1016/j.bbamcr.2004.04.007)
35. Lee K *et al.* 2016 Contribution of actin filaments and microtubules to cell elongation and alignment depends on the grating depth of microgratings. *Nanobiotechnology* **14**, 35. (doi:10.1186/s12951-016-0187-8)
36. Ventre M, Causa F, Netti PA. 2012 Determinants of cell-material crosstalk at the interface: towards engineering of cell instructive materials. *J. R. Soc. Interface* **9**, 2017–2032. (doi:10.1098/rsif.2012.0308)
37. Huveneers S, Oldenburg J, Spanjaard E, van der Krogt G, Grigoriev I, Akhmanova A, Rehmann H, de Rooij J. 2012 Vinculin associates with endothelial VE-cadherin junctions to control force-dependent remodeling. *J. Cell Biol.* **196**, 641–652. (doi:10.1083/jcb.201108120)
38. Prasaina N, Stevensa T. 2009 The actin cytoskeleton in endothelial cell phenotypes. *Microvasc. Res.* **77**, 53–63. (doi:10.1016/j.mvr.2008.09.012)
39. Théry M, Pépin A, Dressaire E, Chen Y, Bornens M. 2006 Cell distribution of stress fibres in response to the geometry of the adhesive environment. *Cell Motil. Cytoskel.* **63**, 341–355. (doi:10.1002/cm.20126)
40. Wolfenson H, Henis Y, Geiger B, Bershadsky AD. 2009 The heel and toe of the cell's foot: a multifaceted approach for understanding the structure and dynamics of focal adhesions. *Cell Motil. Cytoskel.* **66**, 1017–1029. (doi:10.1002/cm.20410)
41. Guo WH, Wang YL. 2012 A three-component mechanism for fibroblast migration with a contractile cell body that couples a myosin II-independent propulsive anterior to a myosin II-dependent resistive tail. *Mol. Biol. Cell.* **23**, 1657–1663. (doi:10.1091/mbc.E11-06-0556
42. Czeisler C, Mikawa T. 2013 Microtubules coordinate VEGFR2 signaling and sorting. *PLoS ONE* **8**, e75833. (doi:10.1371/journal.pone.0075833.)
43. LaValley DJ, Zanotelli MR, Bordeleau F, Wang W, Schwager SC, Reinhart-King CA. 2017 Matrix stiffness enhances VEGFR-2 internalization, signaling, and proliferation in endothelial cells. *Converg. Sci. Phys. Oncol.* **3**, 044001. (doi:10.1088/2057-1739/aa9263)